A novel hybrid approach for automated detection of retinal detachment using ultrasound images

A novel hybrid approach for automated detection of retinal detachment using ultrasound images

Joel En Wei Koh[a], U Raghavendra[b], Anjan Gudigar[b], Ooi Chui Ping[g], Filippo Molinari[f], Samarth Mishra[c], S. Mathavan[c], Rajiv Raman[c], U Rajendra Acharya[a,d,e*]

[a]Department of Electronics and Computer Engineering, Ngee Ann Polytechnic, Clementi 599489, Singapore.
[b]Department of Instrumentation and Control Engineering, Manipal Institute of Technology, Manipal Academy of Higher Education, Manipal 576104, India.
[c] Sankara Nethralaya Chennai-600006, India
[d]Department of Bioinformatics and Medical Engineering, Asia University, Taichung, Taiwan
[e]International Research Organization for Advanced Science and Technology (IROAST) Kumamoto University, Kumamoto, Japan.
[f]Department of Electronics and Telecommunications, Politecnico di Torino, Italy

[g]School of Science and Technology, Singapore University of Social Sciences, 463 Clementi Road, Singapore, 599494, Singapore

*Corresponding Author: aru@np.edu.sg

Abstract

Retinal detachment (RD) is an ocular emergency, which needs quick intervention to preclude permanent vision loss. In general, ocular ultrasound is used by ophthalmologists to enhance their judgment in detecting RD in eyes with media opacities which precludes the retinal evaluation. However, the quality of ultrasound (US) images may be degraded due to the presence of noise, and other retinal conditions may cause membranous echoes. All these can influence the accuracy of diagnosis. Hence, to overcome the above, we are proposing an automated system to detect RD using texton, higher order spectral (HOS) cumulants and locality sensitive discriminant analysis (LSDA) techniques. Our developed method is able to classify the posterior

vitreous detachment and RD using support vector machine classifier with highest accuracy of 99.13 %. Our system is ready to be tested with more diverse ultrasound images and aid ophthalmologists to arrive at a more accurate diagnosis.

Keywords: Retinal detachment, texture, ultrasound, classifier, image, HOS, cumulant

1. Introduction

Retinal detachment (RD) can lead to severe visual impairment and blindness if left untreated [1]. However, early diagnosis and timely treatment can improve visual prognosis. Limited availability of trained retinal specialists in third world countries makes it difficult for early diagnosis of these patients. Ultrasound has been found to be an effective modality for medical personnel who are not retinal specialists, like general ophthalmologists to diagnose RD [2] as well as distinguish RD from a common mimicker and posterior vitreous detachment (PVD) [3]. In opaque ocular media, like significant cataract or vitreous hemorrhage, ultrasound B scan remains as the mainstay for the diagnosis of RD. On ultrasound, RD appears as a membrane of even thickness with uniform high reflectivity, attached to the optic nerve with limited movement on dynamic ultrasound. A similar appearance may be seen in blood-lined PVD which is moderate to highly reflective with good mobility in contrast to poor mobility in RD. Accurately distinguishing between these two conditions can help to provide immediate and correct treatment for RD [3].

Retina is the innermost membrane of the eye on which the lens focuses light, thus forming an image. It is made of light sensitive cells which transmit the optical information to brain in the form of electrical impulses. Retinal detachment is a medical emergency where the retina detaches from its supporting membrane, thus pulling itself out from its normal position. Retinal detachment hinders normal vision, which if left untreated can lead to permanent loss of vision. There are various methods implemented

for the diagnosis of this disorder. The most common and easy one being the ophthalmoscopy. Here, the doctor examines the fundus of the eye with the help of yellow light. The fundus consists of retina, the optic disc and the blood vessels. This technique requires greater amount of examiner experience to correctly detect the disorder [1]. Since this method involves flashing the light into the eyes to see its interior, the opaqueness of vitreous humor; the jelly inside the eye, can hinder the view as it obstructs the light penetration.

For implementing ophthalmoscopy, the pupil needs to be dilated. For this purpose, a medicated eye drop is used. The use of this drop for dilation could be discomforting and may lead to various complications [3]. This is one of the major drawbacks of using this method. There are also other noninvasive tools and techniques for the diagnosis of retinal detachment. MRI (Magnetic Resonance Imaging) [4], OCT (Optical Coherence Tomography) [5], color fundus photography [6] and ultrasound imaging are the commonly used techniques for better diagnosis of this disease [7, 8].

OCT produces high resolution images of the retina. Similar to ultrasound imaging, but instead of sound, the reflected light is used for imaging. The depths in the image is perceived based on the time taken by the light to travel back after reflection. The drawback of this technique is that the equipment is expensive and the light gets scattered off the peripheral parts of the crystalline lens, thus, deteriorating the quality of the image. MRI imaging has the advantage of wide imaging view over the other ocular imaging techniques. Amongst all these methods, ultrasound (US) imaging has a major advantage over other imaging techniques [33 - 41]. Various researchers have proven that ultrasound imaging provides highly sensitive, efficient, accurate and reliable images. However, ultrasound is only used in two scenarios: (a) optical media opacities precluding a view to the retina; (b) personnel untrained in ophthalmoscopy, i.e. non-ophthalmologists, nevertheless this will be less frequent.

Shinar et al. [9] has shown that with the use of ocular ultrasound, less experienced person could detect RD with greater sensitivity and specificity. Study carried out on 35 patients by Coleman et al. [10] showed that ultrasonography is a powerful technique in the diagnosis of RD. In addition, Damianidis, et al. [4] demonstrated that ultrasonography is better than CT and MRI for evaluation of RD. Yuen Aoi Chee et.al [11] worked on various processing tools for retinal detachment from ultrasound imaging. Morajab et.al [12] used principal component analysis (PCA) combined with Hough Transform for feature extraction. Recently, Gupta et al. [42] had proposed a thresholding based technique and concluded that their results matched with radiologists. It was also observed that it was challenging to differentiate PVD from RD using US images.

The main focus of this paper is to develop an efficient system to segregate PVD and RD in all situations. The remainder of the article is presented in the following sections. The details of the data acquisition is given in Section 2. The proposed methodology is outlined in Section 3 and results are presented in Section 4. The discussion on the results are described in Section 5 and conclusion is in Section 6.

2. Dataset used

A total of 100 patients were included in the study, with 36 patients having retinal detachment and 64 patients with blood-lined posterior vitreous detachment (PVD). The diagnosis of retinal detachment or blood lined PVD was done by two independent graders (RRN, SHMA) based on clinical presentation, ultrasonographic feature of aftermovements and membrane reflectivity. Ultrasonography was carried out using Appasamy Marvel B-scan-64-bit system with B-scan probe of 12 MHz and A scan of 10 MHz respectively. The A scan vector was adjusted to pass perpendicular to the retinal detachment or blood lined PVD as required, with an adjustment of the gain between

zero to 20 Decibel. Ultrasonography was performed in supine position for all the patients. Ultrasonography was done in a sitting position wherever a diagnosis of exudative component was suspected and such patients were excluded from the group. In total, we used 229 ultrasound images from 100 patients. Figure 1 shows typical ultrasound images belonging to RD and PVD subjects.

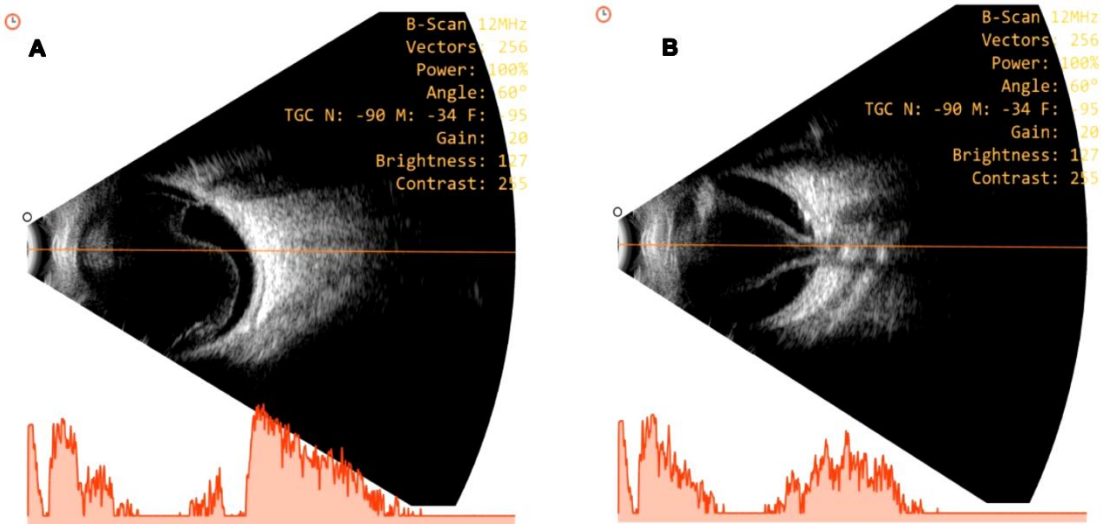

Figure 1. Typical ultrasound images of two classes: (a) RD and (b) PVD.

3. Proposed methodology

Our approach to identify RD requires *three* major stages. In the first stage US images are preprocessed and various filter banks of texton are applied with different scales and orientations to highlight the signatures of retinal structure. In the second stage, retinal features are represented by using higher order spectra (HOS) cumulants and locality sensitive discriminant analysis (LSDA). In the final stage, the features are evaluated statistically and classification is performed using support vector machine (SVM) classifier as given in Figure 2. The details of each stage is given in the following subsequent section.

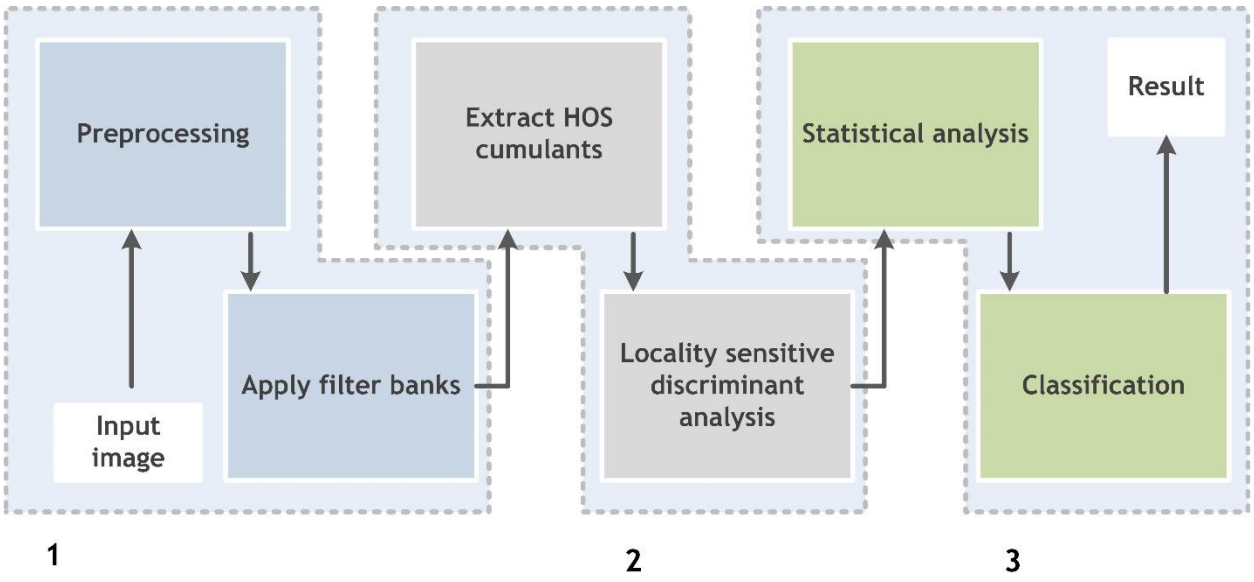

Figure 2: Three-stage architecture of proposed system.

Stage 1: Formation of 2D filtered image

Preprocessing is required to ensure that the dataset is consistent and relevant features are displayed more clearly. To minimize the noise in the input images, adaptive histogram equalization is applied to the gray scale image [13]. This step results in uniform spreading of intensities in the output image and it is rescaled to 368×444 using interpolation technique [14] for further analysis.

Texture analysis refers to the characterization of the regions in an image by their texture content. It attempts to quantify intuitive qualities as a function of spatial variation in pixel intensities. The basic microstructures of images are obtained by using various set of filters. In this study, we have used Leung-Malik (LM) [15], maximum response (MR) [17], and Schmid (S) [16] filter banks to formulate the 2D filtered image.

In practice, convolution operation is performed between input images with filter banks [30, 31, 32]. LM filter bank has a total of 48 filters: derivative of two Gaussian at 3 scales and 6 orientations and 8 and 4 Laplacian of Gaussian and Gaussian filters, respectively. At multiple orientations and scales, LM set has a combination of spot,

edge, and bar filters. Figure 3 shows the example of filtered image after applying LM filter bank to posterior vitreous detachment and retinal detachment. However, MR filter bank comprises of 38 filters which is similar to LM filters. MR8 is obtained to accomplish rotational invariance, which consist of 8 filter response. Subset of MR8 i.e., filter bank MR4 is considered to look at the filter at single scale. In addition, 13 rotationally invariant ("Gabor-like") filters are generated to form S filter bank and these filters have rotational symmetry. Figure 4 and Figure 5 show the example of filtered images after applying MR and S filter banks, respectively for posterior vitreous detachment and retinal detachment classes. These filters are able to capture various salient features at various orientations of the image. The application of these filter banks helps to enhance the 2D singularities such as curves, line, etc. present in the retinal images. This enable us to generate various nonlinear features at different orientations which helps yield highest performance.

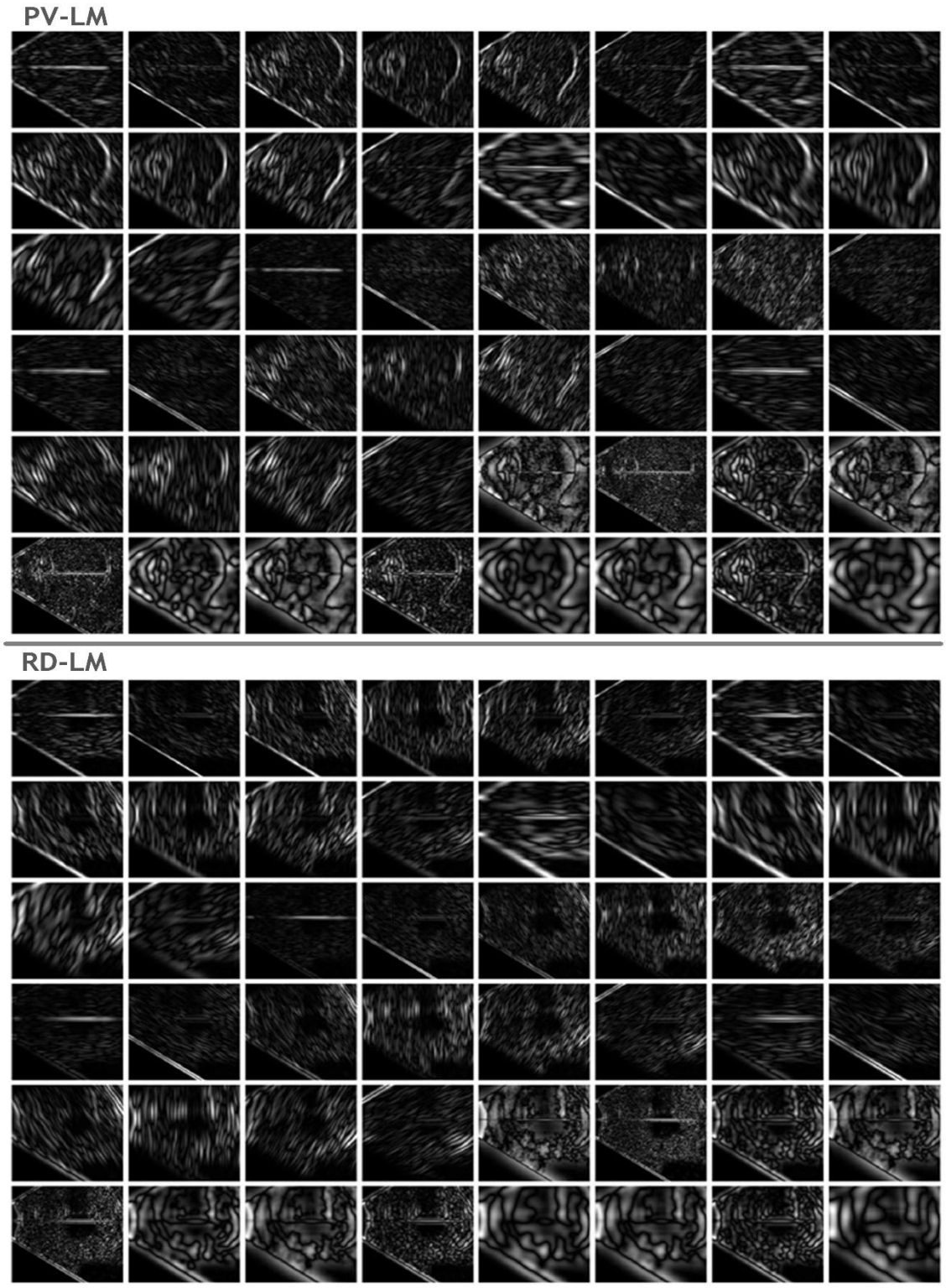

Figure 3: Images obtained after applying LM filter bank to PVD and RD ultrasound images.

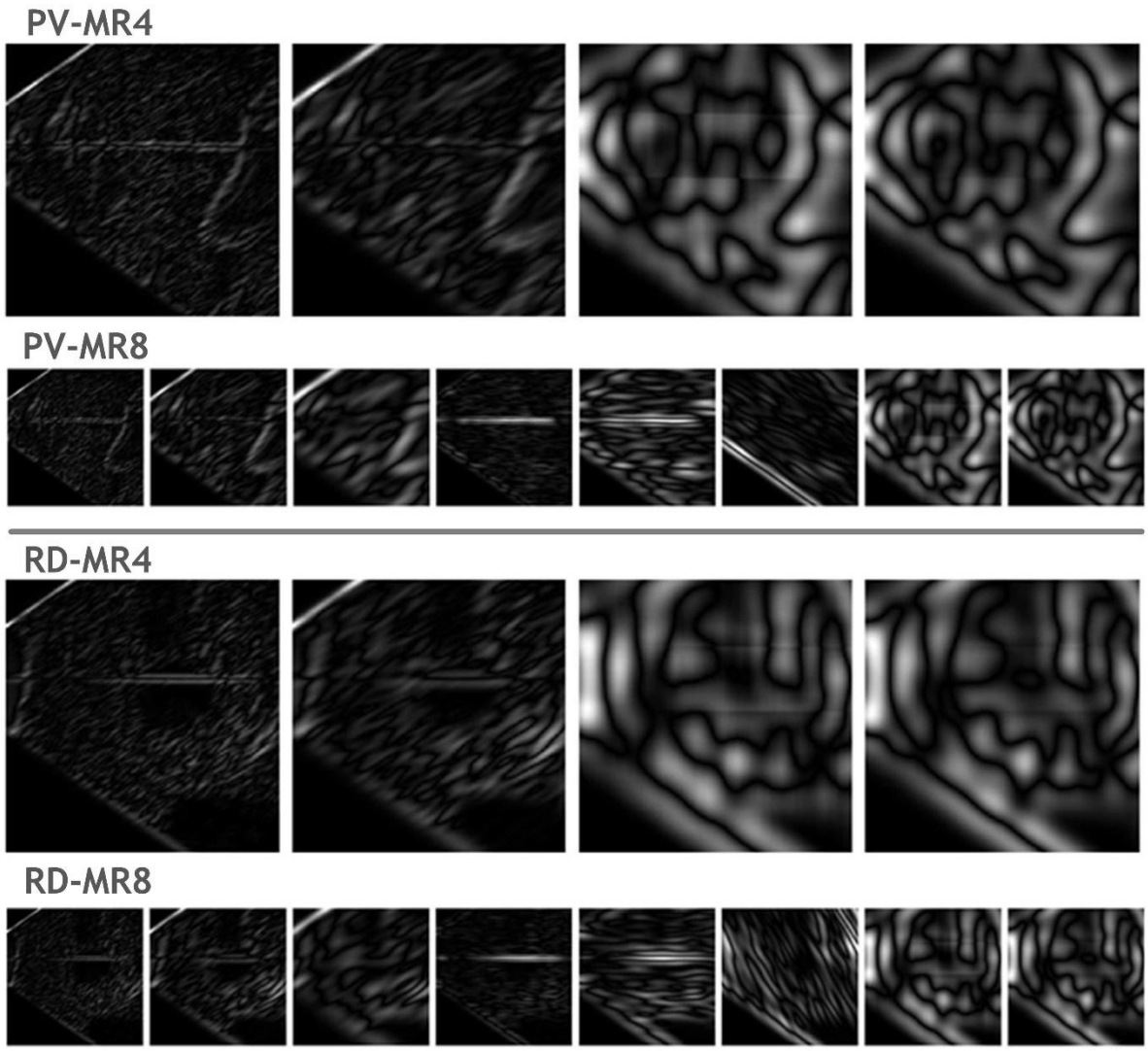

Figure 4: Images obtained after applying MR filter bank to PVD and RD ultrasound images.

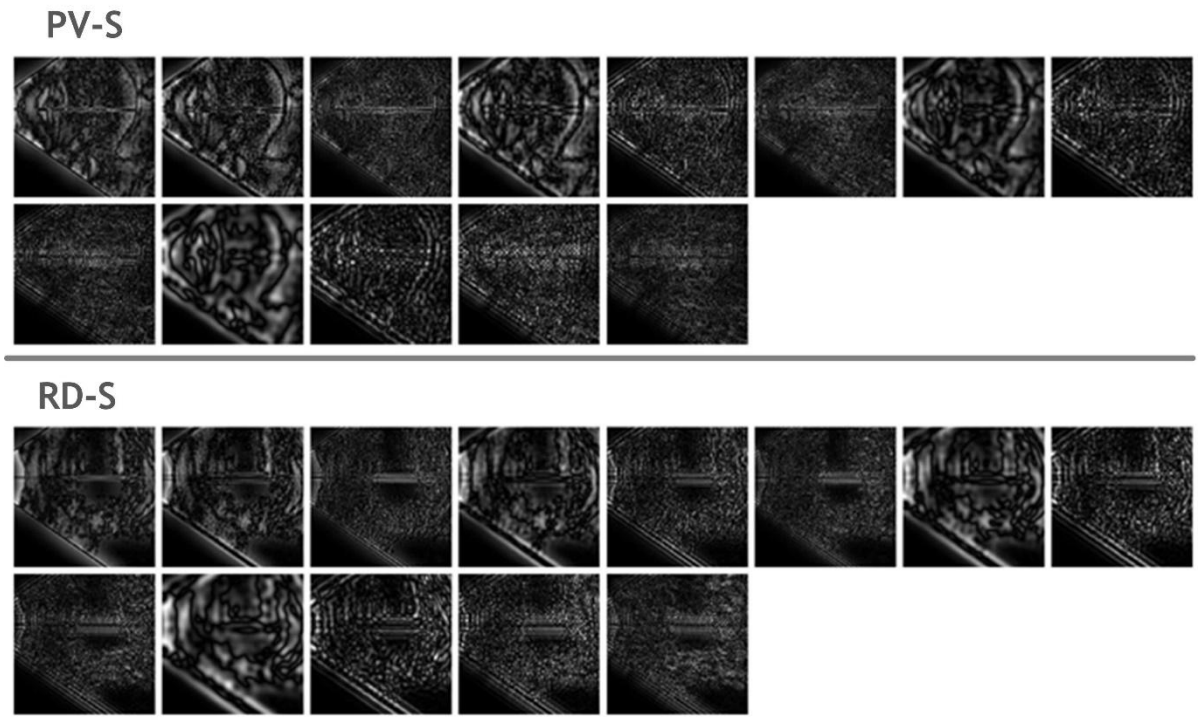

Figure 5: Images obtained after applying S filter bank to PVD and RD ultrasound images.

Stage 2: Representation of retinal images

Since most of the bio-signals are non-Gaussian, non-stationary, and nonlinear in nature, higher order statistics is required to model it. For the given signal, higher order correlations are the HOS cumulants [18,45] and it is derived from the higher order moments. In the present study, 3rd order cumulants are used to analyze the retinal images. Generally, cumulants are estimated in terms of moments [19, 20] and cumulants are most preferable choice for stochastic signals. In order to generate 3rd order cumulants, the knowledge about 1st, 2nd, and 3rd order moments are essential. It is noted that, HOS has shown better performance in the field such as in brain image analysis [21] and thyroid nodules analysis [22]. In practice, 3rd order HOS cumulants are calculated from 1D signals. Therefore, images are converted to one dimensional (1D) projections

with Radon transform (RT) [23]. The HOS cumulants are computed for each 10° i.e. $,0^{\circ}, 10^{\circ}, \ldots\ldots\ldots, 170^{\circ}$.

These features are further reduced to fewer features using LSDA method [29]. It is a geometrically motivated supervised dimensionality reduction technique. Initially a graph is constructed to know the underlying structure of the manifolds. This graph is then divided into between-class and within-class graph using label information (i.e., G_w and G_b). For P data points $\{x_1, x_2, \ldots\ldots\ldots, x_P\} \subset \mathbb{R}^n$, sampled from manifold, the weight matrix (W) is given by,

$$W_{w,ij} = \begin{cases} 1 \; if \; x_i \in K_w(x_j) \; or \; x_j \in K_w(x_i) \\ o \qquad\qquad\qquad\qquad otherwise \end{cases} \tag{1}$$

$$W_{b,ij} = \begin{cases} 1 \; if \; x_i \in K_b(x_j) \; or \; x_j \in K_b(x_i) \\ o \qquad\qquad\qquad\qquad otherwise \end{cases} \tag{2}$$

Where, $K(x_i)$ is the set of k-nearest neighbors and it is further divided to $K_w(x_j)$ or $K_w(x_i)$ if neighbors share the same label and $K_b(x_j)$ or $K_b(x_i)$ if neighbors do not have the same label. The within-class graph experiences a large penalty if x_i and x_j belongs to the same class and are mapped distantly. Likewise, between-class graph experiences a large penalty if x_i and x_j belongs to different class and are mapped nearby. Therefore it is for good mapping of appropriate minimization and maximization of the objective functions.

Stage 3: Identification

In this stage, the class of test image is classified using generated features from the preceding stage. The significance level of these features help us to form the set of important features required to perform the classification. Hence the features are statistically tested using student's t-test [24]. For 2 sets of data, p- and t-values are obtained. The features are ranked based on t-values i.e., $t_1 > t_2 > \ldots\ldots\ldots$, which

indicates that feature with greater t-values are more valued. The features are organized from highest to lowest rank and ignoring lower significant feature will possibly increase the classification accuracy.

These features are further categorized by using various supervised learning classifiers. In the present work, we have used support vector machine (SVM) classifier to separate the two classes. SVM is a binary classifier which generates the hyperplanes to separate the classes [25]. It helps to train more data with higher number of classes quickly and less vulnerable to over fitting compared to other classification techniques [26]. For the unknown sample u decision function of the SVM can be written as,

$$f(u) = sgn(\sum_{j=1}^{N_v} \alpha_j l_j k(v_j, u) + b) \quad (3)$$

where, α_j are the Lagrange multipliers, l_j are labels, $k(v_j, u)$ is the kernel function, v_j are the support vectors, and N_v is the number of support vectors. In this work, order 1, 2, and 3 of polynomial kernel (i.e., P1:SVM, P2:SVM, and P3:SVM) is used.

4. Results

The system was developed and executed using MATLAB platform with standalone system. The images were first preprocessed and resized to predefined size. For each image LM = 48, MR4 = 4, MR8 = 8, and S = 13 filtered images were generated. HOS cumulants for each filtered image was extracted for every10°. Hence, each image produced 117504, 9792, 19584, and 31824 features using LM, MR4, MR8, and S filter coefficients, respectively. Hence, *four* feature sets were generated for PVD and RD images. The size of these features were further reduced to 30 with the help of LSDA data reduction technique. Highest weighted features were then classified using SVM classifier. To validate our approach, 10-fold cross-validation approach wass employed.

The parameters such as true and false positive (i.e., TP and FP) and true and false negative (i.e., TN and FN) were used to estimate the system accuracy (S_{acc}), positive predictive value (S_{ppv}), Sensitivity (S_{sen}), and Specificity (S_{spe}). It is noted that the system achieved highest accuracy of 99.13% using only 10 LSDA features. The Tables 1-4 shows the system performance using various filter coefficients. It is also observed that P3:SVM achieved better result in all cases.

Table 1 : Classification results for LM filter based approach.

Classifier	# features	TP	TN	FP	FN	S_{acc} (%)	S_{ppv} (%)	S_{sen}(%)	S_{spe} (%)
P1:SVM	10	96	127	4	2	97.38	96.00	97.96	96.95
P2:SVM	10	96	131	0	2	99.13	100.00	97.96	100.00
P3:SVM	**10**	**96**	**131**	**0**	**2**	**99.13**	**100.00**	**97.96**	**100.00**

*P1: Polynomial kernel of order 1
P2: Polynomial kernel of order 2
P3: Polynomial kernel of order 3

Table 2 : Classification results for MR4 filter based approach.

Classifier	# features	TP	TN	FP	FN	S_{acc} (%)	S_{ppv} (%)	S_{sen}(%)	S_{spe} (%)
P1:SVM	8	94	129	2	4	97.38	97.92	95.92	98.47
P2:SVM	9	95	129	2	3	97.82	97.94	96.94	98.47
P3:SVM	**9**	**97**	**129**	**2**	**1**	**98.69**	**97.98**	**98.98**	**98.47**

Table 3 : Classification results for MR8 filter based approach.

Classifier	# features	TP	TN	FP	FN	S_{acc} (%)	S_{ppv} (%)	S_{sen}(%)	S_{spe} (%)
P1:SVM	7	68	86	45	30	67.25	60.18	69.39	65.65
P2:SVM	8	73	96	35	25	73.80	67.59	74.49	73.28
P3:SVM	**9**	**78**	**97**	**34**	**20**	**76.42**	**69.64**	**79.59**	**74.05**

Table 4 : Classification results for S filter based approach.

Classifier	# features	TP	TN	FP	FN	S_{acc} (%)	S_{ppv} (%)	S_{sen}(%)	S_{spe} (%)
P1:SVM	13	89	122	9	9	92.14	90.82	90.82	93.13
P2:SVM	16	95	124	7	3	95.63	93.14	96.94	94.66

P3:SVM	**13**	**95**	**131**	**0**	**3**	**98.69**	**100.00**	**96.94**	**100.00**

5. Discussion

All the images were first subjected to various filters of the texton. Each set of output from LM, MR4, MR8, and S were analyzed separately. The HOS cumulants were computed from filtered image. It is observed that LM based images achieved promising results as compared to other filters. The HOS features extracted from LM were discriminative as shown in Figure 6.

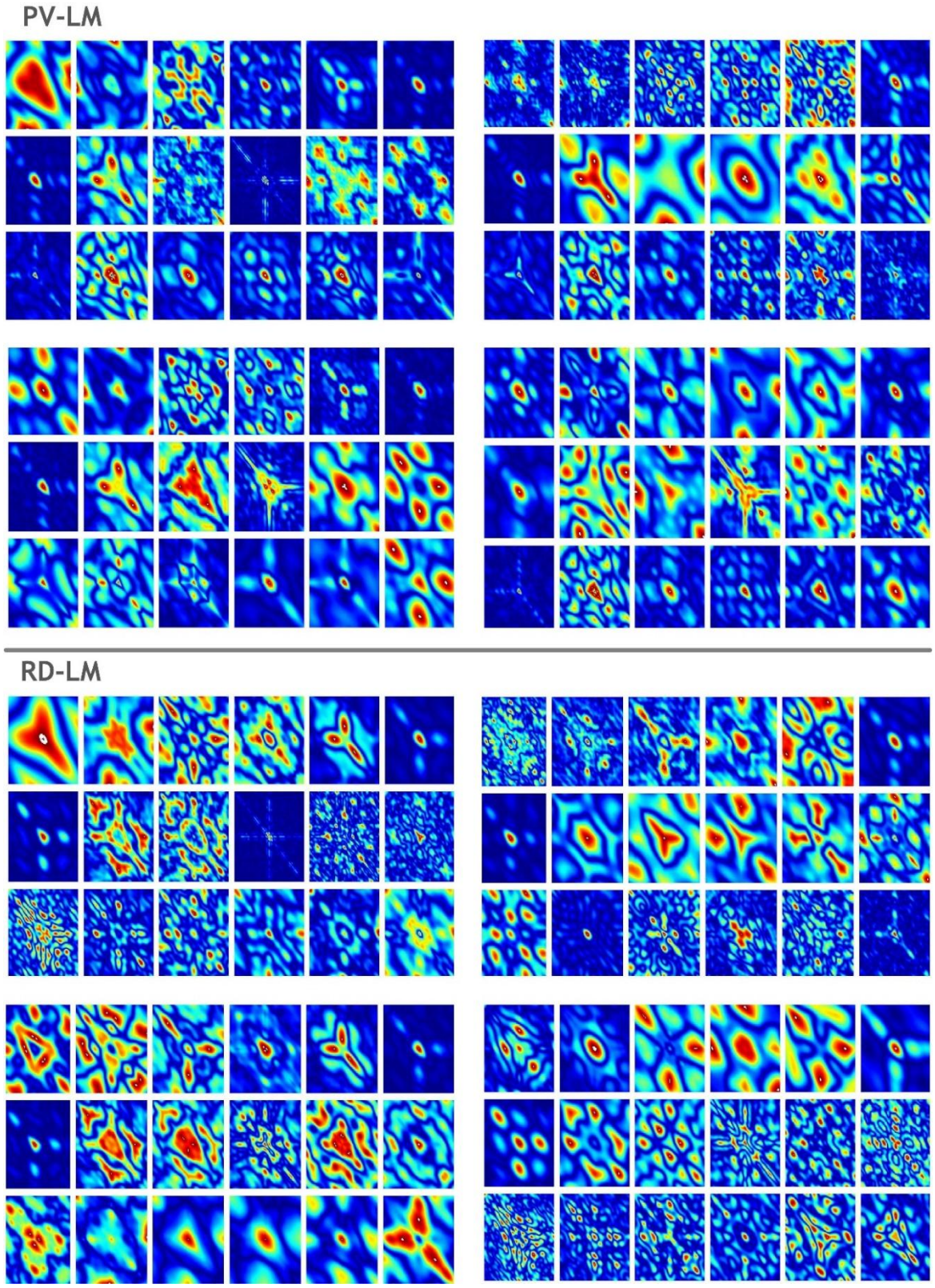
PV-LM
RD-LM

Figure 6. Plots of HOS cumulants at various angles (for LM 1, 4, 8, and 12) for RD and PVD classes

To validate the efficacy of LSDA, the graph was also constructed using neighbouring samples i.e., neighbourhood preserving embedding (NPE) [27]. The principal component analysis (PCA) [28] was also considered for the evaluation, as it preserved the global structure. The total number of significant features (i.e., $p<0.005$) obtained by PCA, NPE, and LSDA were 15, 5, and 11 respectively. Figure 7 shows the plot of system accuracy as a function of number of features. It is observed that PCA achieved maximum S_{acc} of 67.24% , S_{ppv} of 64.93% S_{sen} of 51.02 % and S_{spe} of 79.38 % using 13 features. NPE produced S_{acc} of 65.50% , S_{ppv} of 62.66% S_{sen} of 47.95% and S_{spe} of 78.62% using 5 features. However, S_{acc} of 99.13% , S_{ppv} of 100% S_{sen} of 97.96% and S_{spe} of 100% weres achieved by LSDA using only 10 features.

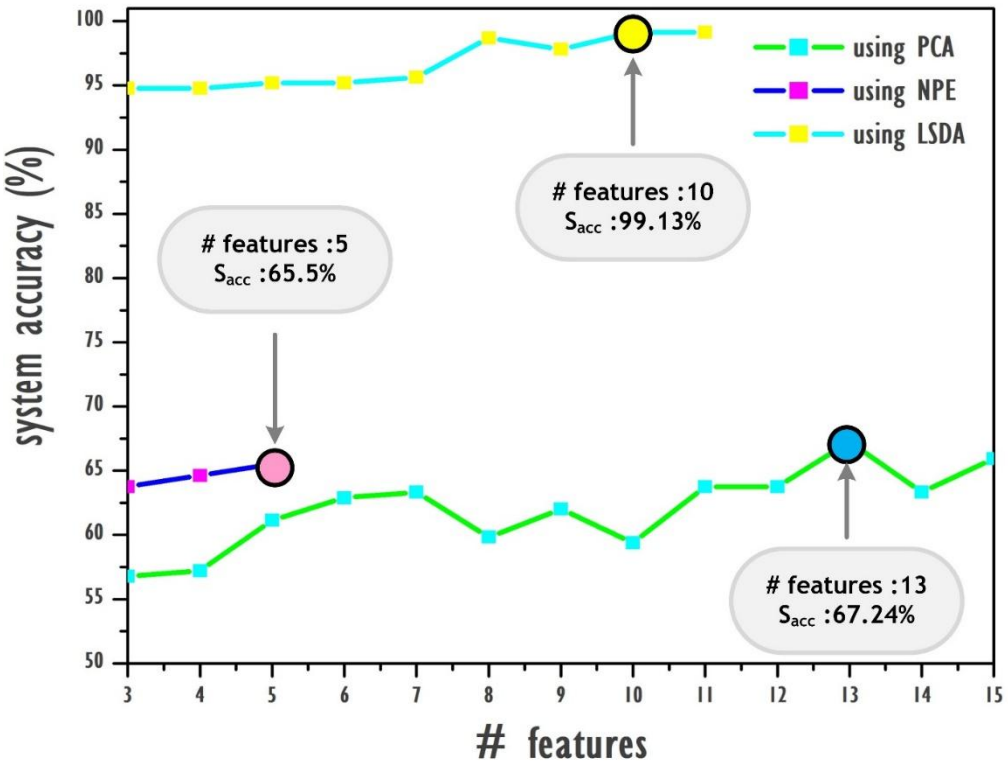

Figure 7: Plot of accuracy versus number of features.

LSDA achieved remarkable performance using only 10 features. The *mean* (m) and standard deviation (s) of initial 5 LSDA features with its t-values are shown in Figure 8. LSDA efficiently handled nonlinearity by producing the discriminative features. It was noted that the *mean* values for PVD were quite high, when compared to RD. The PCA and NPE data reduction techniques are unable to discriminate the nonlinear HOS features. Hence, they gave low system performances.

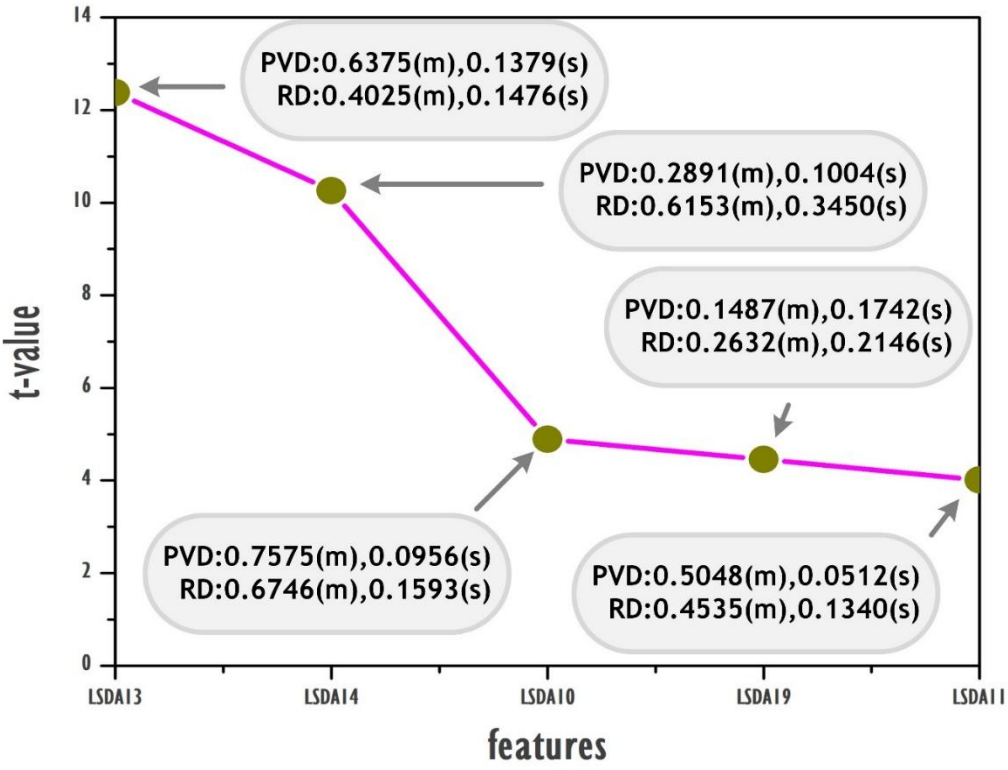

Figure 8: Plot of t-value versus features.

The major advantages of the proposed system are as follows:

1. Various filters of texton, HOS cumulants, textures, and LSDA helped capture very minute changes in the US images.
2. Our system achieved the specificity of 100%, i.e., all PVDs were properly classified by the system automatically, which could reduce the workload of clinicians by 50%.

3. Our system obtained highest accuracy (99.13%) using only *ten* features. Hence, our system is less complex and easy to implement.
4. The proposed method can also be applied to other image modalities like fundus, optical coherence tomography (OCT), Heidelberg Retina Tomograph (HRT), and magnetic resonance images of the eye.

Application of texton, higher order spectral (HOS) cumulants and locality sensitive discriminant analysis (LSDA) techniques for automated detection of retinal detachment using ultrasound (US) images is the novelty of this paper. To the best of our knowledge, we are the first group to develop the automated system for retinal detachment using US images. The main technical contribution of this paper are: texton, HOS cumlants and data reduction techniques. The proposed method is able to capture subtle changes like retinal detachments efficiently and hence yielded high performance.

The limitation of this work is that, we have only used 100 subjects in this study. In future, we intend to use large database to develop the deep learning model like convolutional neural network [43,44] for automated diagnosis of retinal detachment. Such developed models may also be used for the diagnosis of other eye diseases like cataract, glaucoma and choroidal lesions.

6. Conclusion

Here, a novel system able to automatically discriminate PVD and RD using ultrasound (US) images has been developed. The novelty of this system is the use of filters, HOS cumulants and LSDA. The HOS features were able to capture the minute changes present in the US images and yielded highest classification accuracy of 99.13 % using only *ten* features. HOS cumulants were robust to noise present in the US images. This distinction would assist the ophthalmologists to give better and more accurate

treatments to their patients. In future, we plan to test our developed model using more US images before installing for clinical use.

Reference

1. Ohsugi, H., Tabuchi, H., Enno, H. and Ishitobi, N. (2017). Accuracy of deep learning, a machine-learning technology, using ultra–wide-field fundus ophthalmoscopy for detecting rhegmatogenous retinal detachment. *Scientific Reports*, 7(1).
2. Shinar, Z., Chan, L. and Orlinsky, M. (2011). Use of Ocular Ultrasound for the Evaluation of Retinal Detachment. *The Journal of Emergency Medicine*, 40(1), pp.53-57.
3. Baker, N., Amini, R., Situ-LaCasse, E., Acuña, J., Nuño, T., Stolz, U. and Adhikari, S. (2018). Can emergency physicians accurately distinguish retinal detachment from posterior vitreous detachment with point-of-care ocular ultrasound?. *The American Journal of Emergency Medicine*, 36(5), pp.774-776.
4. Damianidis, C. H., et al. "Magnetic Resonance Imaging and Ultrasonographic Evaluation of Retinal Detachment in Orbital Uveal Melanomas." The neuroradiology journal 23.3 (2010): 329- 338.
5. Jaffe, Glenn J., and Joseph Caprioli. "Optical coherence tomography to detect and manage retinal disease and glaucoma." American journal of ophthalmology 137.1 (2004): 156-169.
6. Subhadra Jalali Smt. Kumari Santhamma Retinal detachment' Community Eye Health Vol 16 No. 46 2003
7. Blumenkranz, Mark S., and Sandra Frazier Byrne. "Standardized echography (ultrasonography) for the detection and characterization of retinal detachment." Ophthalmology 89.7 (1982): 821-831.
8. Kahn, Andy, et al. "Retinal Detachment diagnosed by bedside ultrasound in the emergency department." The California Journal of emergency medicine 6.3 (2005): 47.
9. Shinar, Zachary, Linda Chan, and Michael Orlinsky. "Use of ocular ultrasound for the evaluation of retinal detachment." The Journal of emergency medicine 40.1 (2011): 53-57.
10. Coleman, D. Jackson, and Robert L. Jack. "B-scan ultrasonography in diagnosis and management of retinal detachments." Archives of ophthalmology 90.1 (1973): 29-34.
11. Yuen Aoi Chee, et al. "Image Processing Analysis for Ultrasound Retinal Detachment Images." Advances in Environment, Biotechnology and Biomedicine ISBN: 978-1-61804-122-7.
12. Sona Morajab, Soheyl Zarkandy, "An Intelligent Method Based OnHough Transform and Support Vector Machine to Diagnose Retinal Detachment in Ultrasound Images" International Research Journal of Engineering and Technology (IRJET), Volume: 02 Issue: 09 Dec-2015

13. S. M. Pizer et al., ``Adaptive histogram equalization and its variations,''Comput. Vis., Graph., Image Process., vol. 39, no. 3, pp. 355368, 1987.
14. T. Blu, P. Thevenaz, M. Usner, Linear interpolation revitalized, IEEE Transactions on Image Processing 13 (May (5)) (2004).
15. T. Leung and J. Malik, ``Representing and recognizing the visual appearance of materials using three-dimensional textons,'' Int. J. Comput. Vis., vol. 43, no. 1, pp. 29-44, Feb. 2001.
16. L. Zhang, X. Ye, T. Lambrou, W. Duan, N. Allinson, and N. J. Dudley,``A supervised texton based approach for automatic segmentation and measurement of the fetal head and femur in 2D ultrasound images,'' Phys. Med. Biol., vol. 61, no. 3, pp. 1095-1115, Feb. 2016.
17. J.-M. Geusebroek, A. W. M. Smeulders, and J. van de Weijer, ``Fast anisotropic Gauss ltering,'' IEEE Trans. Image Process., vol. 12, no. 8, pp. 938-943, Aug. 2003.
18. J.M. Mendel, Tutorial on higher-order statistics (spectra) in signal processing and system theory: theoretical results and some applications, Proceedings of the IEEE 79 (1991) 278–305.
19. Brillinger DR, Rosenblatt M. Computation and interpretation of k-th order spectra. In: Harris B, editor. Spectral analysis of time series. New York: Wiley; 1967.p. 189–232.
20. Nikias CL, Raghuveer MR. Bispectrum estimation—a digital signal processing framework. Proceedings of the IEEE 1987;75:869–91.
21. A. Gudigar, U. Raghavendra, E. J. Ciaccio, N. Arunkumar, E. Abdulhay and U. R. Acharya, "Automated Categorization of Multi-Class Brain Abnormalities Using Decomposition Techniques With MRI Images: A Comparative Study," in IEEE Access, vol. 7, pp. 28498-28509, 2019.
22. U. Raghavendra , Anjan Gudigar , M. Maithri , Arkadiusz Gertych , Kristen M. Meiburger , Chai Hong Yeong , Chakri Madla , Pailin Kongmebhol , Filippo Molinari , Kwan Hoong Ng , U. Rajendra Acharya, Optimized multi-level elongated quinary patterns for the assessment of thyroid nodules in ultrasound images, Computers in Biology and Medicine 95 (2018) 55–62
23. S.R. Deans , Hough transform from the Radon transform, IEEE Trans. Pattern Anal. Mach. Intell. 3 (2) (1981) 185–188.
24. Student t-test, Last Accessed: 11.10.2019. [Online]. Available: http://www.physics.csbsju.edu/stats/t-test.html
25. Burges CJC (1998) A tutorial on support vector machines for pattern recognition. Data Min Knowl Disc 2(2):121–167
26. Greenhalgh J, Mirmehdi M (2012) Real-time detection and recognition of road traffic signs. IEEE TransIntell Transp Syst 13(4):1498–1506
27. X. He, Deng Cai, S. Yan, H.J. Zhang, Neighborhood preserving embedding, in: Proc. of the 10th IEEE International Conference on Computer Vision, 2005a, pp. 1208–1213
28. M. Turk, A. Pentland, Eigenfaces for recognition, Journal of Cognitive Neuroscience 3 (1) (1991) 71–86.

29. Deng Cai, Xiaofei He, Kun Zhou, Jiawei Han, Hujun Bao, Locality sensitivediscriminant analysis, Proceedings of the 20th International Joint Conference on Artificial Intelligence IJCAI'07 (2007) 708–713.
30. U Rajendra Acharya, Shreya Bhat, Joel EW Koh, Sulatha V Bhandary, Hojjat Adeli, A novel algorithm to detect glaucoma risk using texton and local configuration pattern features extracted from fundus images, Computers in biology and medicine, 8, pp. 72-83, 2017.
31. U Rajendra Acharya, Kristen M Meiburger, Joel En Wei Koh, Edward J Ciaccio, N Arunkumar, Mee Hoong See, Nur Aishah Mohd Taib, Anushya Vijayananthan, Kartini Rahmat, Farhana Fadzli, Sook Sam Leong, Caroline Judy Westerhout, Angela Chantre-Astaiza, Gustavo Ramirez-Gonzalez, A Novel Algorithm for Breast Lesion Detection Using Textons and Local Configuration Pattern Features With Ultrasound Imagery, IEEE Access, 7, pp. 22829-22842, 2019.
32. U Rajendra Acharya, U Raghavendra, Joel EW Koh, Kristen M Meiburger, Edward J Ciaccio, Yuki Hagiwara, Filippo Molinari, Wai Ling Leong, Anushya Vijayananthan, Nur Adura Yaakup, Mohd Kamil Bin Mohd Fabell, Chai Hong Yeong, Automated detection and classification of liver fibrosis stages using contourlet transform and nonlinear features, Computer methods and programs in biomedicine, Vol. 166, Pages. 91-98, 2018.
33. Filippo Molinari, U Raghavendra, Anjan Gudigar, Kristen M Meiburger, U Rajendra Acharya, An efficient data mining framework for the characterization of symptomatic and asymptomatic carotid plaque using bidimensional empirical mode decomposition technique, Medical & biological engineering & computing, 2018.
34. U Rajendra Acharya, U Raghavendra, Joel EW Koh, Kristen M Meiburger, Edward J Ciaccio, Yuki Hagiwara, Filippo Molinari, Wai Ling Leong, Anushya Vijayananthan, Nur Adura Yaakup, Mohd Kamil Bin Mohd Fabell, Chai Hong Yeong, Automated detection and classification of liver fibrosis stages using contourlet transform and nonlinear features, Computer Methods and Programs in Biomedicine, Vol. 166, pp. 91-98, 2018.
35. U Rajendra Acharya, Ayesha Akter, Pradeep Chowriappa, Sumeet Dua, U Raghavendra, Joel EW Koh, Jen Hong Tan, Sook Sam Leong, Anushya Vijayananthan, Yuki Hagiwara, Marlina Tanty Ramli, Kwan Hoong Ng, Use of Nonlinear Features for Automated Characterization of Suspicious Ovarian Tumors Using Ultrasound Images in Fuzzy Forest Framework, International Journal of Fuzzy Systems, Springer, Vol. 20, No. 4, Pages: 1385-1402, 2018.
36. Kristen Meiburger, Massimo Salvi, Maurizio Giacchino, U Acharya, Marco Minetto, Cristina Caresio, Filippo Molinari, Quantitative analysis of patellar tendon abnormality in asymptomatic professional "Pallapugno" players: A texture-based ultrasound approach, Applied Sciences, 8(5), pp. 660.
37. Filippo Molinari, U. Raghavendra, Anjan Gudigar , Kristen M. Meiburger, U. Rajendra Acharya, An Efficient Data Mining Framework for the Characterization of

Symptomatic and Asymptomatic Carotid Plaque using Bidimensional Empirical Mode Decomposition Technique, Medical and Biomedical Engineering & Computing, Springer, Vol. 56, No. 9, pp. 1579–1593, 2018.

38. U Raghavendra, Hamido Fujita, Anjan Gudigar, Ranjan Shetty, Krishnananda Nayak, Umesh Pai, Jyothi Samanth, U Rajendra Acharya, Automated technique for coronary artery disease characterization and classification using DD-DTDWT in ultrasound images, Biomedical Signal Processing and Control, Elsevier, Vol. 40, Pages. 324-334, 2017.
39. U Raghavendra, U Rajendra Acharya, Anjan Gudigar, Jen Hong Tan, Hamido Fujita, Yuki Hagiwara, Filippo Molinari, Pailin Kongmebhol, Kwan Hoong Ng, Fusion of spatial gray level dependency and fractal texture features for the characterization of thyroid lesions, Ultrasonics, Elsevier, 202-210, 2017.
40. U Raghavendra, U Rajendra Acharya, Anjan Gudigar, Ranjan Shetty, N Krishnananda, Umesh Pai, Jyothi Samanth, Chaithra Nayak, Automated screening of congestive heart failure using variational mode decomposition and texture features extracted from ultrasound images, Neural Computing and Applications, Springer, 28 (10), Pages: 2869–2878, 2017.
41. U Rajendra Acharya, U Raghavendra, Hamido Fujita, Yuki Hagiwara, Joel EW Koh, Tan Jen Hong, Vidya K Sudarshan, Anushya Vijayananthan, Chai Hong Yeong, Anjan Gudigar, Kwan Hoong Ng, Automated Characterization of Fatty Liver Disease and Cirrhosis Using Curvelet Transform and Entropy Features Extracted from Ultrasound Images, Computers in Biology and Medicine, Elsevier, Vol. 79, Pages: 250-258, 2016.
42. Rajeev Gupta, Pramod Kumar Singh, Basant Kumar, Abhishek Singh, Ayushi Chandra, Automated Detection of Retinal Detachment from Ocular Ultrasound using Image Thresholding, 5th International Conference on Signal Processing and Integrated Networks (SPIN), 2018.
43. R Acharya, YKE Ng, JS Suri, Image modeling of the human eye, Artech House, 2008.
44. JH Tan, H Fujita, S Sivaprasad, SV Bhandary, AK Rao, KC Chua, U. R. Acharya, Automated segmentation of exudates, haemorrhages, microaneurysms using single convolutional neural network, Information sciences, 420, 66-76,2017.
45. RJ Martis, UR Acharya, CM Lim, KM Mandana, AK Ray, C Chakraborty, Application of higher order cumulant features for cardiac health diagnosis using ECG signals, International journal of neural systems 23 (04), 1350014, 2013.